



Development of selective laser melting irregular open-cell titanium lattice structure to mimic the human cancellous bone

Vasily A. Bautin^{1,3} · Ilya V. Bardin^{1,3} · Artem V. Yudin^{2,3} · Evgeny V. Svistunov³ · Vyacheslav E. Bazhenov¹ · Ruslan A. Rytov¹

Received: 20 July 2020 / Accepted: 9 April 2022 / Published online: 29 April 2022
© The Author(s), under exclusive licence to Springer Nature Switzerland AG 2022

Abstract

Open-cell titanium lattice structures produced by selective laser melting (SLM) are attractive for creation of patient-specific implants with high level of bone ingrowth. In this work, irregular SLM lattice structures made of titanium (cp-Ti) with an average beam thickness of 300 μm and an average porous size of 600 μm were investigated. Optimal processing conditions of SLM for obtaining irregular open-cell cp-Ti lattice structures with mechanical and porous geometry close to human cancellous bone were developed. It was observed that the main parameter of SLM affected on beam thickness is volumetric energy density. Influence of orientation of cubic samples on the construction platform (on the plane, on the edge or on the corner) on properties of lattice structures was investigated. The corner orientation was found to be optimal. It was shown that chemical etching is effective post-treatment method for obtaining required beam thickness and removing the attached powder particles. Optimal chemical etching conditions are the following: etching solution contains 30 mL HNO_3 + 45 mL HF + 120 mL water, etching time is 10 s. The elastic modulus and the elastic limit of etched lattice samples are 1.4–1.9 GPa and 44–51 MPa, respectively, which correlates with characteristics of human cancellous bone. Compression of samples during mechanical tests occurred without beams destruction. Corrosion characteristics of obtained etched and non-etched lattice structures in Hank's Balanced Salt Solution (HBSS) have been improved compared with cp-Ti bulk samples. The biological and medical tests of the obtained samples will be carrying out to determine biocompatibility, influence on the growth of bone tissue, permeability, etc.

Keywords Titanium · Selective laser melting · Cancellous bone · Lattice structure · Mechanical properties · Biomedical application

1 Introduction

The two main specifications for successful long-term orthopedic implantation are known [1–3]: (1) mechanical properties of implant are close to bone tissues; (2) intensive bone ingrowth existence. The spongy tissue found in bone interior

(human cancellous bone) has low elastic modulus: from 0.02 to 5 GPa [1]. As the elastic modulus of a bulk metallic alloy is considerably higher, production of different lattice structures made of these alloys allows to reduce the elastic modulus difference. In addition, open-cell porous architectures are promising for effective bone ingrowth [1].

Lattice structures are topologically ordered, three-dimensional open-celled patterns composed of one or more repeating unit cells [4, 5]. The most interesting method of obtaining such products made from titanium alloys is one of the types of additive manufacturing (AM), namely, selective laser melting (SLM) or laser powder bed fusion (L-PBF). A comprehensive review of SLM made lattice structures can be found in [4]. The ability to produce high-quality complex shape metallic components makes SLM perfect for the fabrication of medical patient-specific implants. Moreover, the stiffness of AM lattice

✉ Vasily A. Bautin
bautin@list.ru

¹ National University of Science and Technology «MISiS»,
119049 Moscow, Russian Federation

² National Research Nuclear University MEPhI,
115409 Moscow, Russian Federation

³ State Research Center of the Russian Federation, Central
Mechanical Engineering Research Institute, Research
and Production Association, Joint-Stock Company
(CNIITMASH JSC), 115088 Moscow, Russian Federation

structures is closer to that of bone. The latter property is very promising for biomedical applications [4].

Mullen et al. [6] found typical specification for structures suitable for application in orthopedic surgery: pore size range: 450–600 μm ; porosity range: $65\% \pm 5\%$; compressive strength: 40 MPa. They used relatively simple single octahedral unit cell to produce pure titanium lattice structures by SLM.

It is worth noting that creation of titanium SLM made lattice structures has several specific aspects:

- discrepancies between CAD models and as fabricated geometry [4]

Van Bael et al. [7] noticed an increase in beam thickness up to 112 μm compared to the designed thickness (100 μm) for lattice samples produced from Ti6Al4V powder using laser power of 42 W, scanning velocity of 260 mm/s and the powder layer thickness of 30 μm . These authors have shown that the main reason for this behavior is a large melt pool size of 180 μm .

Pyka et al. [8] also reported increasing in the beam thickness of the as-produced SLM-Ti6Al4V structures compared to the designed thickness.

- surface roughness due to attachment of the powder particles [4, 9]

It was shown [8], that the staircase effect enhances the powder particle attachment to the beam bottom section, which introduces the heterogeneity of the surface topology of the SLM manufactured samples. One of the ways for removing attached powder particles is post-treatment, for example, chemical etching (CHE). For chemical etching of titanium alloys, different solutions based on HF acid have been used [8]. An increase of the HF concentration resulted in a more effective removal of the attached particles, especially when it combined with longer treatment duration [8].

- only regular open-cell titanium lattice structures were well studied

There are three the main types of regular lattice structures [4]: (1) strut-based lattice structures, such as body-centred cubic (BCC), face-centred-cubic (FCC), BCC and FCC with z-struts (BCCZ and FCCZ) [10], cubic [11], and diamond [12]; (2) lattice structures with triply periodic minimal surfaces (TPMS) cells [13, 14] and (3) shell lattices [15]. We would like to note that a possibility of using irregular open-cell

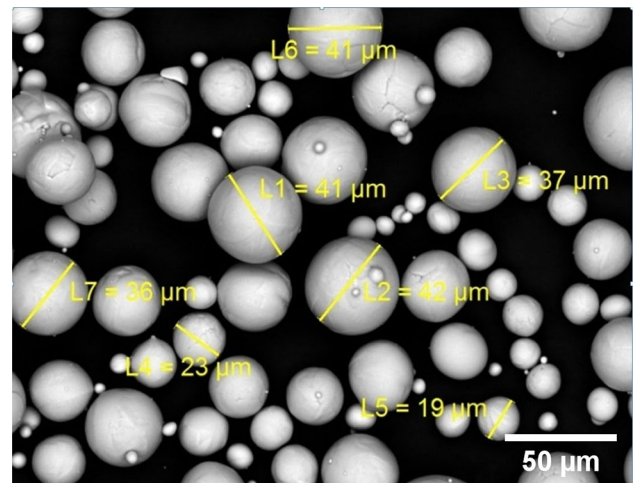


Fig. 1 SEM micrograph of VT1-00 titanium powder

titanium lattice structures for medical implants is still not well investigated.

In this paper, we study SLM made irregular open-cell commercially pure titanium (cp-Ti) lattice structures that mimic the human cancellous bone. Optimal processing conditions of SLM for obtaining such structures with mechanical and porous geometry close to human cancellous bone were determined. Also, the optimal processing conditions of chemical etching for removing attached powder particles were found. The obtained etched and non-etched lattice cp-Ti samples have satisfactory corrosion properties in Hank's Balanced Salt Solution (HBSS) at 37 °C.

2 Materials and methods

Commercially available gas-atomized cp-Ti (Russian alloy VT1-00) powder with a spherical morphology produced in VIAM (www.viam.ru) was used in this work. The nominal chemical composition of VT1-00 alloy is shown in Table 1. A particle size is in a range of 9–55 μm (Fig. 1), an average particle size is 35 μm . Figure 2 shows an SEM micrograph illustrating the powder size and morphology.

The manufacturing of the samples was performed using self-developed MeltMaster^{3D}-550 (CNIITMASH JSC; location: CNIITMASH) machine with parameters shown in Table 2.

The obtained titanium samples with dimension 10 × 10 × 10 mm had an irregular (random) structure with an average beam thickness of 300 μm and an average porous size of 600 μm . Note that an average porous size

Table 1 Nominal chemical composition (wt.%) of VT1-00 alloy

Ti	Si	Fe	O	H	N	C	Others
Base	0.08	0.15	0.10	0.008	0.04	0.05	0.10

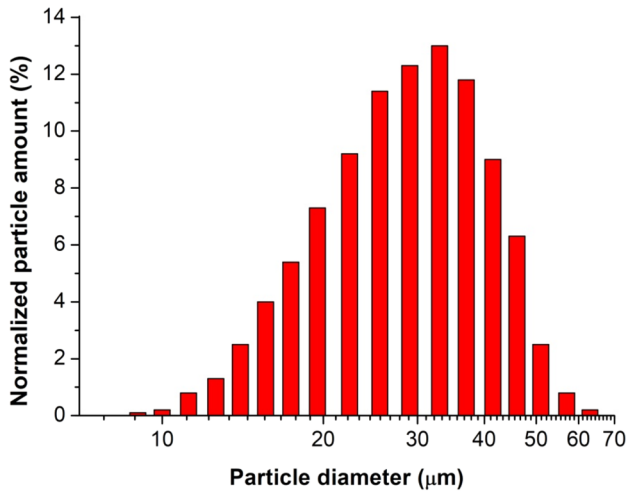


Fig. 2 Distribution of particles size of VT1-00 titanium powder

is the midpoint of the triangle height. Special self-made software was used for creation of 3D model. When optimizing the topology, the following parameters were varied: beam thickness, average distance between beams, and angle between beams with a range of $50^\circ \pm 5^\circ$. The main optimization parameter was the average distance between the beams, equal to $600 \mu\text{m}$. Also despite the presence of an irregularity, topology optimization had several rules:

- the nodes in the vertices of cube have 6 beams;
- the nodes on the edges of cube have 4–12 beams;
- the nodes on the faces of cube have 10–12 beams.
- the nodes filling the inner cube space have 14 or 16 beams.

Samples were obtained at various process parameters of SLM and different orientations as shown in Fig. 3. To analyze and select the optimal processing conditions for producing a lattice structure with minimal deviations of the pore size and beam thickness from those specified in the 3D model, SLM parameters such as: laser power in the range from 130 to 280 W, scanning speed from 550 mm/s up to 750 mm/s and hatch distance from 100 to 120 μm were varied. Laser spot diameter was $90 \mu\text{m}$. SLM was carried out at a powder layer thickness of $50 \mu\text{m}$ in an argon atmosphere with a residual oxygen content of less than 800 ppm.

A simple linear one-pass unidirectional scanning strategy was used as shown in Fig. 4. The pattern was rotated from layer to layer by 60 degrees.

The morphology of the powder particles and lattice structures were investigated using a high-resolution scanning electron microscope JEOL 6610L (JEOL Ltd; location: CNIITMASH) with an energy dispersive X-ray spectroscopy (EDS) attachment JED-2300.

Compression tests of titanium lattice specimens were carried out in accordance with ISO 13314 using Makron

Table 2 Parameters of MeltMaster^{3D}-550 machine

Dimensions of work space	600 × 450 × 550 mm
Maximum power of laser/type of laser	1000 W/Yb-fiber Laser
Construction rate	15–70 cm ³ /h
Powder layer thickness	20–250 μm
Laser spot diameter	90–700 μm
Maximum scanning speed	10 m/s
Inert gas consumption while operating of machine	5 L/min
Inert gas consumption while ventilation of machine	100 L/min
Oxygen content	Less than 800 ppm
Pressurized air	30 L/min, 6–8 atm

Special gear with diameter 115 mm was used for reducing the work space

Fig. 3 3D models of lattice cp-Ti structures planning for SLM creation. **a** sample grown on the edge; **b** sample grown on the corner; **c** sample grown on a plane

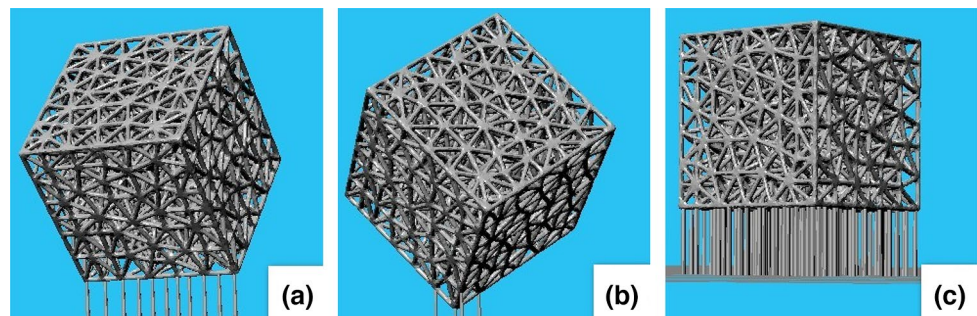
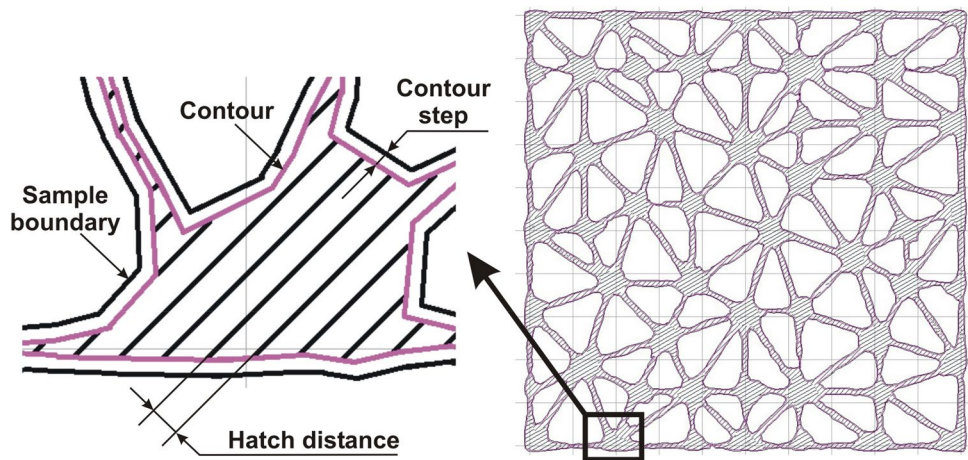


Fig. 4 Scanning strategy of the one of the layers of lattice cp-Ti structure



universal servo-hydraulic testing machine UT-02-0025 (ITW India Private Limited—BISS Division; location: CNIITMASH). Compression tests were carried out under continuous monotonic loading to a maximum load of $P=25$ kN. The speed of movement of the active capture was 1 mm/min. Compression diagrams of the tested samples were constructed in the coordinates $\sigma - \epsilon$, where $\sigma = P/A$ is the conditional stress determined by the standard formula for calculating stresses for materials with a continuous structure (P is the compression load, kN, A is the initial cross-sectional area of the sample, mm^2), ϵ – compressive strain (%).

To remove the attached powder particles, chemical etching (CHE) was used. Lattice cubic samples were etched by immersion in an aqueous solution contained HNO_3 and HF acids under constant stirring. The etching solution composition is as follows: 30 mL nitric acid (60–70% HNO_3), 45 mL hydrofluoric acid (more than 60% HF) and distilled water of 90 or 120 mL. Etching time was 5, 10, 15, 20 and 30 s.

The electrochemical corrosion behavior of etched and non-etched lattice samples and cp-Ti bulk sample were performed using the IPC Pro MF (NTF Volta LLC; location: NUST “MISI”) potentiostat in Hank’s Balanced Salt Solution (HBSS) at 37 °C. Bulk sample was cut from disk made of alloy VT1-00 according GOST 26492–85 [16] and was not etched. Samples was mounted in epoxy resin and polished using 600 grit SiC abrasive paper. The samples working area was calculated using ImageJ Software. HBSS (volume of 1L) contains 8 g NaCl, 400 mg KCl, 140 mg CaCl_2 , 100 mg $\text{MgSO}_4 \cdot 7\text{H}_2\text{O}$, 100 mg $\text{MgCl}_2 \cdot 6\text{H}_2\text{O}$, 120 mg $\text{Na}_2\text{HPO}_4 \cdot 12\text{H}_2\text{O}$, 60 mg KH_2PO_4 , 1 g D-Glucose, 350 mg NaHCO_3 . A three-electrode system was employed in which the samples served as working electrode. Platinum and Ag/AgCl electrodes were used as the counter and reference electrodes, respectively. Potentiodynamic polarization curve were measured from the cathodic to the anodic region with a scan rate of 1 mV/s. The corrosion current density and corrosion potential were determined from Tafel fitting.

The experiments were carried out several times for standard statistical data processing. For compression and electrochemical tests, the typical curves was chosen.

3 Results and discussion

Power of laser, P (W), scanning speed, v (mm/s), hatch distance, h (mm), and layer thickness, L_t (mm) was used to calculate volumetric energy density E_v (J/mm^3) [9] as a critical parameter for determination of an optimal processing conditions:

$$E_v = \frac{P}{vL_t h}$$

Figure 5 shows effect of E_v on the beam thickness in the vertical (XZ or YZ) and scanning (XY) planes for sample grown on a plane. It was found that the excess E_v leads to the melting of the powder and appearing of the fused material in the lower layers, which leads to broadening of the beams in the vertical plane (XZ or YZ). On the other hand, it was observed that the E_v practically does not affect the size of the beams in the scanning plane (XY plane), and a decreasing of laser power below 160 W leads to the formation of defects on the surface of the struts. For further studies, five types of samples were selected, described in the Table 3.

SEM micrographs of beams and pores of the samples grown on a plane are presented in the Appendix A (Supplementary Materials). The results of measurements of the sizes of the beams of the lattice structures of various samples are given in Table 4. It was found that at the same laser power the beam thickness is higher than those specified on the 3D model at the scanning speed of 650 mm/s. However, at the scanning speed of 750 mm/s, an opposite effect was observed, i.e. the beam thickness is lower. Therefore, optimal processing conditions correspond to laser power

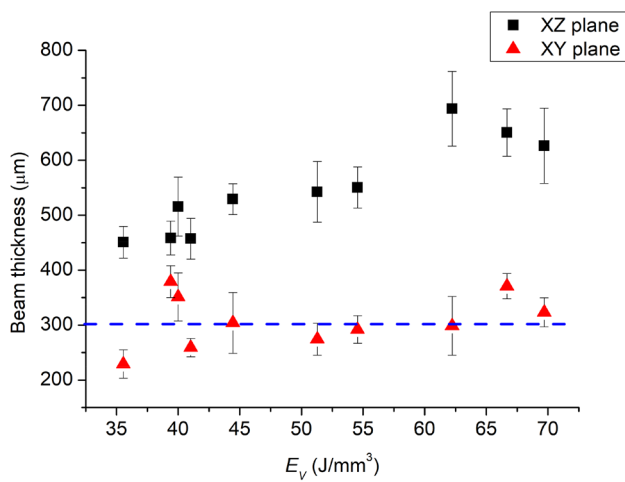


Fig. 5 Effect of volumetric energy density on the beam thickness (samples grown on a plane). Beam thickness from CAD model is shown as blue dash line

of 160 W and scanning speed of 700 mm/s. In addition, the changing of technological conditions does not ensure the absence of attached powder particles on the surface of beams.

According to the optimal processing conditions, samples with different orientations on the construction platform (on the plane, on the edge, and on the corner) were obtained. They are shown in Fig. 6. Samples are contacted with the platform through supports, as Fig. 3 shows.

SEM micrographs of lattice structures produced under optimal processing conditions of SLM with different orientations of samples on the construction platform are presented in the Appendix B (Supplementary Materials). It was observed that the dimensions of the beams of lattice structures exceed the specified values according to the 3D model, but at the same time, the overall deviation of the sizes is the smallest one for the corner orientation relative to the others. Similarly, the difference in size in the “XZ” (or “YZ”) and “XY” planes is the smallest one for the corner orientation. Here and below, the planes are indicated in quotation marks, since for samples grown on an edge and on a corner, the cube faces are located at an angle to the Z

Table 3 Adjusted parameters of SLM used to obtain samples with cp-Ti lattice structures

Sample type	Power of laser, W	Scanning speed, mm/s	Hatch distance, µm	Contour step, µm	Number of contours
I	160	700	120	60	1
II	200				
III	160	650			
IV	160	750			
V	200				

direction. Therefore, the main reason for obtaining beams uniform in thickness for a sample grown on an angle is a more symmetric arrangement of the cube faces relative to vertical direction of growth. Also, orientation on the corner is optimal due to presence of minimum number of support structures. There are some problems with removing the support structures from the lattice samples and the fewer there are, the less possible damage to the samples when removing the supports.

After CHE post-treatment the beam thickness was decreasing (Table 5) and attached powder particles were removed (Fig. 7). A more concentrated etchant (30 mL HNO₃ + 45 mL HF + 90 mL water) does not provide the required etching quality. At short etching times (5 s) in this solution, only the outer beams of the lattice structures are thinned, while attached powder particles remain inside the sample (Fig. 7a). On the other hand, an increase in the etching time to 10 and 15 s leads to the formation of “pits” in the beams with significant thinning (Fig. 7b, c). Therefore, for further studies, a less concentrated etchant was used.

In less concentrated etching solution (30 mL HNO₃ + 45 mL HF + 120 mL water) at etching time of 5 s attached powder particles was observed (See Appendix C), which shows the need for a further increasing of the etching time. However, if the etching time exceeds 15 s significant dissolution of the beam material and their local thinning to 100 µm was observed. Therefore, it was found that the most suitable etching time for the samples studied is 10 s. Etching technology developed provides the necessary dimensions and quality of beams for any orientation of the lattice

Table 4 The sizes of the beams of the lattice structures obtained for different processing conditions shown in the Table 3

Sample type	An average beam thickness in vertical plane (XZ, YZ), µm	An average beam thickness in horizontal plane (XY), µm	Beam thickness from CAD model, µm
I	471.8 ± 44.4	262.3 ± 20.6	300
II	575.0 ± 70.4	325.2 ± 12.5	
III	470.2 ± 43.4	343.8 ± 18.3	
IV	476.0 ± 51.7	279.8 ± 14.3	
V	515.0 ± 52.0	352.7 ± 12.7	



Fig. 6 Photo of the cp-Ti lattice samples grown on the platform in the plane, edge and corner orientations (from left to right)

samples during construction. It gives also a uniformity of the etching inside the sample.

The lattice structures produced by means of optimal processing conditions at different (edge and corner) sample

orientations on the platform were mechanically tested. Compression tests of samples grown on the edge were carried out as shown in Fig. 8. For samples grown on the corner, any specific compression direction during mechanical testing was not used due to symmetry of sample relatively growing direction (Z axis).

The results of mechanical compression tests of cp-Ti lattice structures without and after CHE are presented in Table 6. Table 6 shows the data on the current contraction ΔL_c and the relative contraction ε_c of the samples with a cellular structure measured during loading at a load of 50 N, as well as the calculated values of the absolute ΔL_c and relative ε_c contraction measured after this load was stopped.

Typical compression diagrams both for non-etched and etched samples with a lattice structure are shown in Fig. 9. These dependences are similar to those obtained on samples with a continuous structure made of a plastic material. One can see in Fig. 9 that there are two main stages of deformation under compression, i.e. the stage of elastic deformation and that of plastic deformation. Moreover, the $\sigma - \varepsilon$ diagram has a smooth shape. It means that the beams are deformed without destruction.

There is a non-linear section at the initial stage of loading due to partly uniform fit of the contacting surfaces of the sample and grips of testing machine. In this regard, the

Table 5 The beams thickness (“XY” plane, sample on the corner) of the lattice structures obtained under optimal SLM parameters after CHE

Solution	Etching time, s	An average beam thickness, μm	Beam thickness according to CAD model, μm
30 mL HNO_3 + 45 mL HF + 90 mL water	5	416.8 ± 70.5	300
	10	278.2 ± 69.3	
	15	265.2 ± 87.8	
30 mL HNO_3 + 45 mL HF + 120 mL water	5	428.8 ± 77.5	
	10	370.0 ± 57.8	
	15	349.4 ± 27.2	
	20	329.8 ± 16.0	
	30	204.1 ± 50.4	

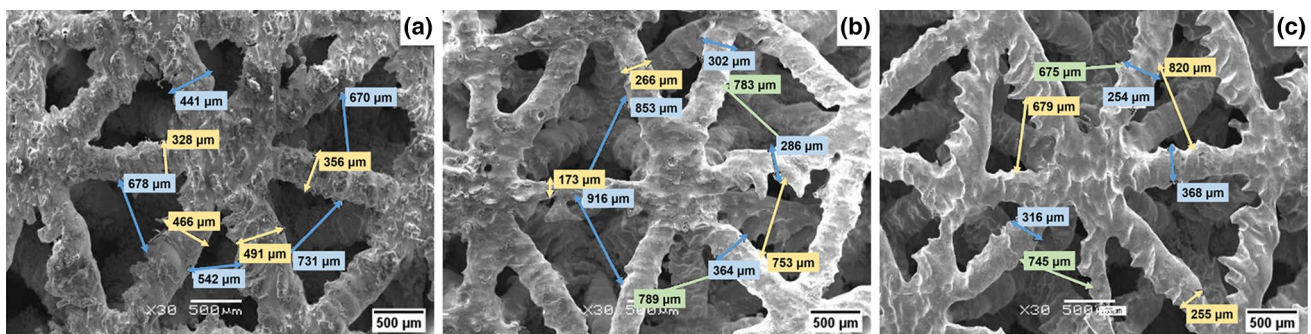


Fig. 7 SEM micrographs of cp-Ti lattice structures produced under optimal processing conditions of SLM after CHE in 30 mL HNO_3 + 45 mL HF + 90 mL water during 5 (a), 10 (b) and 15 (c) s. (“XY” plane, sample on the corner)

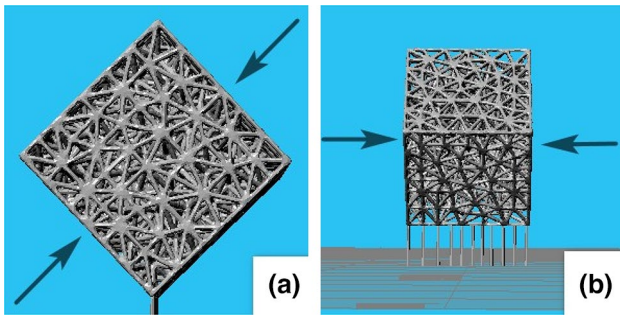


Fig. 8 3D models of samples with a lattice structure indicating the direction of compression: Z' (a) and (XY)' (b)

most objective integral indicators of the sample deformation are the absolute ΔL_c and relative constriction ϵ_c , measured after unloading.

The elastic modulus and the elastic limit of etched samples is lower by 15–20% and 14–19%, respectively, compared to non-etched samples. At the same time, the calculated values of the deformation characteristics of the compression of the etched and non-etched samples have similar values, their differences amount to thousandths of a millimeter at a load of 50 N, i.e. they are at the level of measurement error.

A detailed analysis showed that for some samples additional shear deformation occurs during loading, which leads to decreasing the value of elastic limit of the structure. In the absence of additional shear deformation, the elastic limit is higher than 50 MPa.

The elastic modulus (1.4–1.9 GPa) and the elastic limit (44–51 MPa) of etched lattice samples correlate with characteristics of human cancellous bone and close to structures with Neovius and Gyroid TPMS geometry with relative density (ρ/ρ_s) 0.30–0.32 [1].

Figure 10 shows electrochemical behavior of etched and non-etched cp-Ti lattice samples obtained under optimal processing conditions of SLM and CHE, as well as cp-Ti bulk sample, in HBSS at 37 °C. All samples are in passive state and value of corrosion current density is low as presented in Table 7. Anodic and cathodic curves of etched

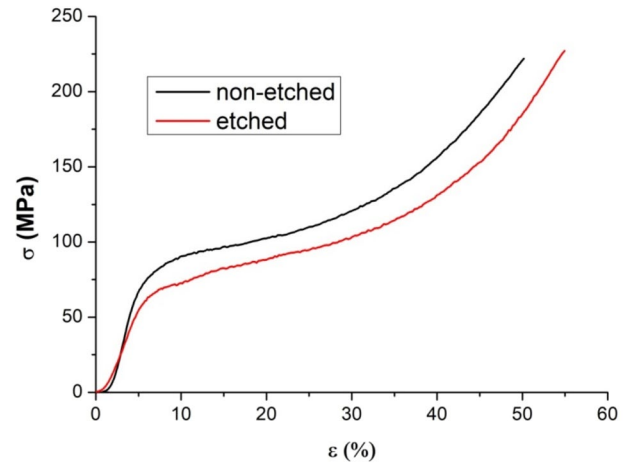


Fig. 9 Typical compression diagrams for non-etched and etched samples with a lattice structure

and non-etched SLM made cp-Ti samples are practically the same, excepting trans-passive region. Cp-Ti bulk sample has more negative corrosion potential and higher value of corrosion current density as shown in Fig. 10 and Table 7. The possible reason of this behavior is different microstructure of SLM made and bulk samples.

4 Conclusions

In summary, the following results have been obtained in the present study:

- (1) The optimal processing conditions of SLM for obtaining irregular open-cell titanium lattice structures with mechanical and geometrical properties close to human cancellous bone were developed:

- Power of laser, W: 160
- Scanning speed, mm/s: 700
- Hatch distance, μm : 120
- Contour step, μm : 60
- Layer thickness, μm : 50

Table 6 The mechanical properties of the cp-Ti lattice structures obtained under optimal SLM parameters without and after CHE at different sample orientation on the platform

Orientation of sample	Compression direction	CHE	Elastic modulus E , GPa	σ_y , MPa	ΔL_c , mm	ϵ_c , %	ΔL_c , mm	ϵ_c , %
On the edge	Z'	-	1.80	58.50	0.079	0.75	0.003	0.03
	(XY)'	+	1.41	50.50	0.024	0.24	0.003	0.03
		-	2.31	53.75	0.053	0.49	0.002	0.02
On the corner	-	+	1.85	44.25	0.039	0.38	0.002	0.02
		-	2.12	58.75	0.037	0.36	0.002	0.02
		+	1.79	47.50	0.013	0.09	0.003	0.03

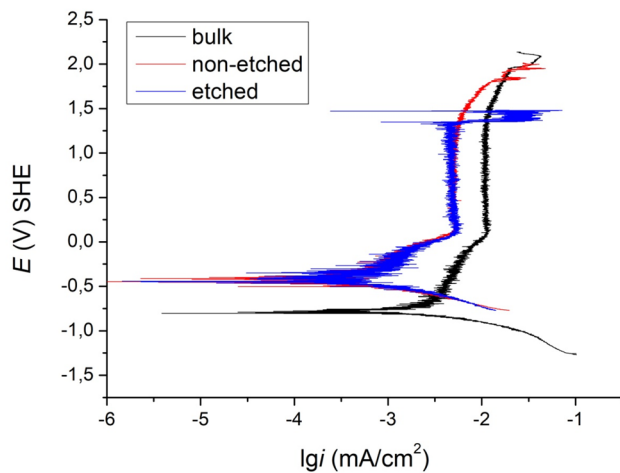


Fig. 10 Electrochemical behavior of different cp-Ti samples in HBSS at 37 °C

It has been established that the volumetric energy density significantly effects on the thickness of the beams in the vertical plane (ZX or ZY) of sample. On the other hand, the dimensions of the beams in the scanning plane (XY) are practically independent of the volumetric energy density.

- (2) It has been found that the optimal orientation of sample on the construction platform is on the corner of sample. In this case, minimum number of supports is used and properties of sample are symmetric relatively growing Z direction.
- (3) Chemical etching is effective post-treatment method for obtaining required beam thickness and removing the attached powder particles. It has been determined that the optimal chemical etching conditions are as follows: etching solution 30 mL HNO₃ + 45 mL HF + 120 mL water, etching time of 10 s.
- (4) Compression diagrams of lattice structures studied are similar to those of continuous structures made of a plastic material. Deformation of beams occurred without destruction. The elastic modulus and the elastic limit of etched lattice samples is 1.4–1.9 GPa and 44–51 MPa, respectively, that correlates with characteristics of human cancellous bone.
- (5) Corrosion current density of etched and non-etched SLM made cp-Ti samples is lower than these for bulk cp-Ti sample and has appropriate level for human implants. In this work, only stiffness was taken into account in the mimic process, therefore, research will be continued in the direction, including biological and medical tests of the obtained samples in order to determine biocompatibility, the effect on bone tissue growth, permeability, etc.

Table 7 Corrosion potential and corrosion current density calculated from Taffel plots (Fig. 10)

Sample	Corrosion potential, V SHE	Corrosion current density, mA/cm ²
SLM etched	-0.45	4.6·10 ⁻⁴
SLM non-etched	-0.45	5.4·10 ⁻⁴
Bulk	-0.78	1.9·10 ⁻³

Supplementary Information The online version contains supplementary material available at <https://doi.org/10.1007/s40964-022-00303-9>.

Acknowledgements The authors wish to acknowledge the financial support of the Ministry of Education and Science of the Russian Federation in the framework of Increase Competitiveness Program of NUST «MISIS», contract № K2-2019-012, K2A-2019-034.

References

1. Alabort E, Barba D, Reed RC (2019) Design of metallic bone by additive manufacturing. *Scripta Mater* 164:110–114
2. Sumner DR (2015) Long-term implant fixation and stress-shielding in total hip replacement // *J Biomech* 48(5):797–800
3. Ryan G, Pandit A, Panagiotis AD (2006) Fabrication methods of porous metals for use in orthopaedic applications // *Biomaterials* 27(13):2651–2670
4. Maconachie T, Leary M, Lozanovski B, Zhang X, Qian Ma, Faruque O, Brandt M (2019) SLM lattice structures: properties, performance, applications and challenges. *Mater Des* 183:108137
5. Zadpoor AA (2019) Mechanical performance of additively manufactured meta-biomaterials // *Acta Biomater* 85:41–59
6. Mullen L, Stamp RC, Brooks WK, Jones E, Sutcliffe CJ (2009) Selective Laser Melting: a regular unit cell approach for the manufacture of porous, titanium, bone in-growth constructs, suitable for orthopedic applications. *J Biomed Mater Res B Appl Biomater* 89(2):325–334. <https://doi.org/10.1002/jbm.b.31219>
7. Van Bael S, Kerckhofs G, Moesen M, Pyka G, Schrooten J, Kruth JP (2011) Micro-CT-based improvement of geometrical and mechanical controllability of selective laser melted Ti6Al4V porous structures. *Mater Sci Eng, A* 528(24):7423–7431
8. Pyka G, Kerckhofs G, Papantoniou I, Speirs M, Schrooten J, Wevers M (2013) Surface roughness and morphology customization of additive manufactured open porous Ti6Al4V structures. *Materials* 6:4737–4757
9. McMillan M, Leary M, Brandt M (2017) Computationally efficient finite difference method for metal additive manufacturing: a reduced-order DFAM tool applied to SLM. *Mater Des* 132:226–243
10. Mazur M, Leary M, McMillan M, Sun S, Shidid D, Brandt M (2019) 5 - Mechanical properties of Ti6Al4V and AlSi12Mg lattice structures manufactured by Selective Laser Melting (SLM). In: Brandt M (ed) *Woodhead Publishing Series in Electronic and Optical Materials, Laser Additive Manufacturing*. Woodhead Publishing, pp 119–161
11. Amin YS, Ahmadi SM, Wauthle R, Pouran B, Schrooten J, Weinans H, Zadpoor AA (2015) Relationship between unit cell type and porosity and the fatigue behavior of selective laser melted meta-biomaterials. *J Mech Behav Biomed Mater* 43:91–100

12. Ahmadi SM, Campoli G, Amin YS, Sajadi B, Wauthle R, Schrooten J, Weinans H, Zadpoor AA (2014) Mechanical behavior of regular open-cell porous biomaterials made of diamond lattice unit cells. *J Mech Behav Biomed Mater* 34:106–115
13. Ataee A, Li Y, Brandt M, Wen C (2018) Ultrahigh-strength titanium gyroid scaffolds manufactured by selective laser melting (SLM) for bone implant applications. *Acta Mater* 158:354–368
14. Zadpoor AA (2015) Bone tissue regeneration: the role of scaffold geometry. *Biomater Sci* 3(2):231–245
15. Tancogne-Dejean T, Diamantopoulou M, Gorji MB, Bonatti C, Mohr D (2018) 3D Plate-lattices: an emerging class of low-density metamaterial exhibiting optimal isotropic stiffness. *Adv Mater* 30(45):1803334
16. GOST 26492–85. Titanium and titanium alloys rolled bars. Specifications. Approved: USSR State Committee for Standards 3/25/1985, p 32

Publisher's Note Springer Nature remains neutral with regard to jurisdictional claims in published maps and institutional affiliations.